Supporting Information

Rationally designed 3D N-doped graphene with holey structure as a bifunctional electrode for sensitive methyl parathion detection and supercapacitors

Shusheng Xu[a], Peijie Wang[a], Mengru Huang[a], Min Hong[b], Yan Zhang[a, *], Chen Su[c], Xue-Rong Shi[a, *]

[a] School of Materials Engineering, Shanghai University of Engineering Science, Shanghai 201620, China
[b] Frontiers Science Center for Transformative Molecules, School of Chemistry and Chemical Engineering, Shanghai Jiao Tong University, Shanghai 200240, China
[c] School of Advanced Materials and Nanotechnology, Xidian University, Xi'an 710071, Shanxi, China

Email: yanzhang@sues.edu.cn, shixuer05@mails.ucas.ac.cn

Materials

L-ascorbic acid, hydrogen peroxide solution (H_2O_2, 30%), urea, $NaNO_3$ and Na_2CO_3 were purchased from Aladdin Industrial Co. Ltd (Shang Hai, China). P-nitrophenol, KCl, $K_3[Fe(CN)_6]$, $K_4[Fe(CN)_6]$, KH_2PO_4 and K_2HPO_4 were bought from Sinopharm Chemical Reagent Co. Ltd. Methyl parathion solution (1000 μg ml^{-1}) was bought from Sigma-Aldrich (USA). Graphene oxide (GO) was prepared by a modified Hummers method. The chemicals were analytical grade, and Ultrapure water (18.2 M Ω cm) were used in all experiments.

Preparation of 3d-G

L-ascorbic acid (100 mg) was dissolved in 10 ml of GO (2 mg ml^{-1}) by ultrasonication for 15 min. The as-obtained suspension was then heated at 90 °C for 2 h. The as-prepared 3d-G hydrogels were immersed in ultrapure water for 2 h to remove excessive L-ascorbic acid.

Instruments

The morphology of 3d-NHG was obtained using scanning electron microscopy (SEM, Zeiss Ultra 55) and transmission electron microscopy (TEM, FEI Tecnai F20). The chemical structures of samples were characterized by X-ray photoelectron spectroscopy (XPS, An AXIS Ultra spectrometer, Kratos Analytical, Ltd.) and Raman spectra (a LabRAM HR Evolution spectrometer, Horiba; laser excitation at 532 nm). The electrochemical experiments were executed using electrochemical workstation (CHI 660C, Shanghai Chen Hua Co. Ltd, China), except Electrochemical impedance spectroscopy (EIS) measurement (a VersaSTAT 4 potentiostat galvanostat, Princeton Applied Research). All electrochemical experiments were performed on a three-electrode system.

Electrochemical tests include cyclic voltammetry (CV) curves at different scan rates, constant current charge/discharge (GCD) curves at different current densities, and electrochemical impedance spectroscopy (EIS) at frequencies of 0.01−100 kHz was performed to estimate the electrochemical performance of as-prepared electrode

materials. The software Zview and equivalent circuit was employed to fit the specific resistance value.

Electrochemical calculation

The specific capacitance (C_s, F g^{-1}) was calculated from the discharge curves using the following equations.

$$C_S = \frac{I \Delta t}{m \Delta V}$$

(1)

Where C_s (F g^{-1}) stand for the specific capacitance, I (A) is the current, Δt (s) is the discharge time, and Δm (g) is the mass loading of active materials.

Calculation details

The generalized gradient approximation of Perdew-Burke-Ernzerhof functional is employed.[1] The K points of 2 × 2 × 1 and 1 × 2 × 1 are employed for the geometry optimization of the 7 × 7 bulk and slab phases, respectively. For the DOS calculation, the K points are increased to 8 × 8 × 1. In addition to a ~30 Å vacuum layer along the z direction, for the model with the hole, the same thickness of vacuum layer is added along x direction to model the edge of the hole. All electrons method is used to treat the core electrons in the same manner as valence electrons. Smearing vale of 0.002 Ha is employed. For geometry optimizations, the energy and force convergence criteria are 1 × 10^{-5} Ha and 0.002 Ha $Å^{-1}$, respectively.

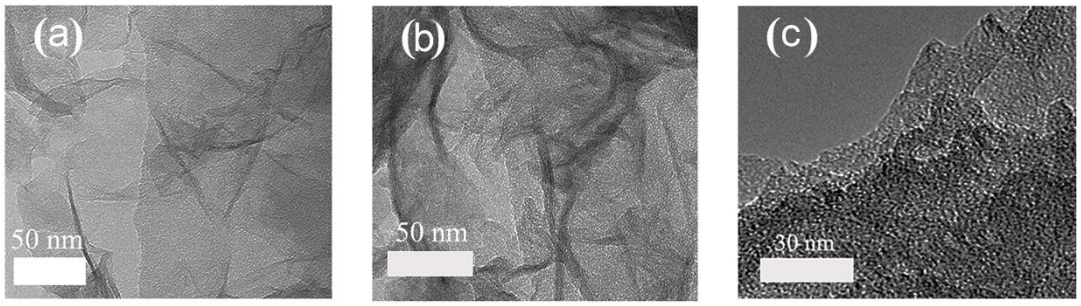

Figure S1 TEM:(a) 3d-G; (b) 3d-NG; (c) 3d-HG

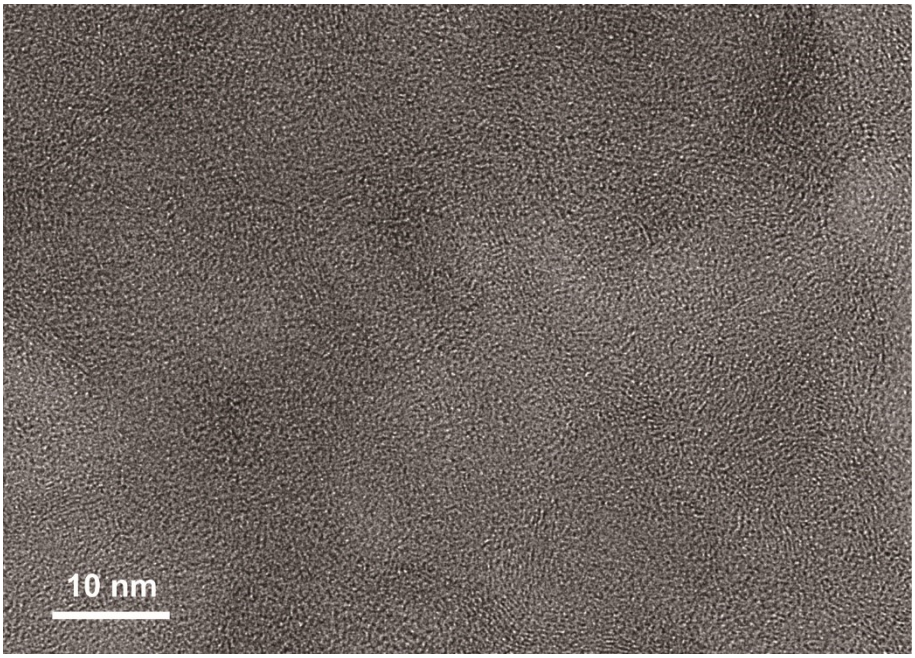

Figure S2. HRTEM of 3d-NG

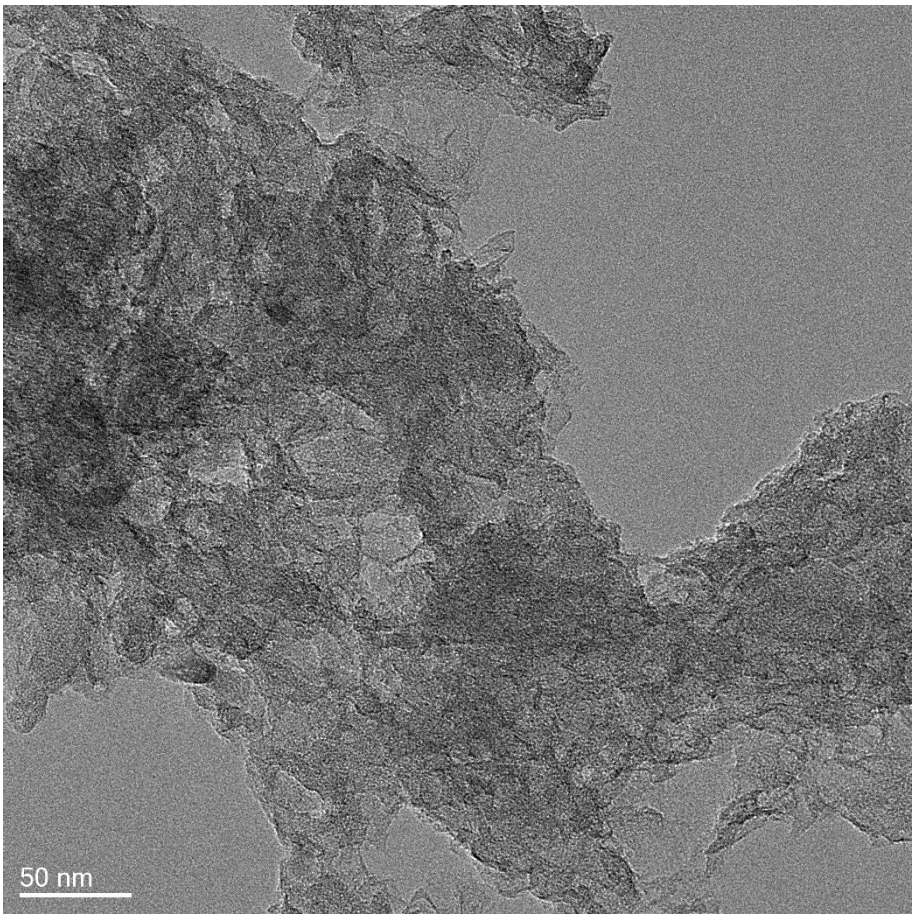

Figure S3. TEM image of 3d-NHG.

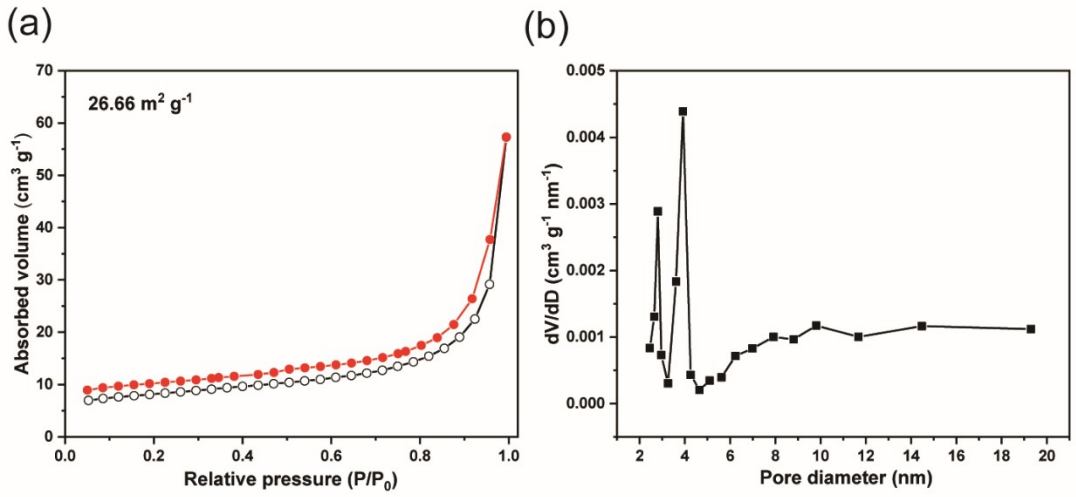

Figure S4. (a) Nitrogen adsorption/desorption isotherms measured at 77 K, (b) Pore distributions calculated from the desorption branch of N2 desorption of 3d-NHG.

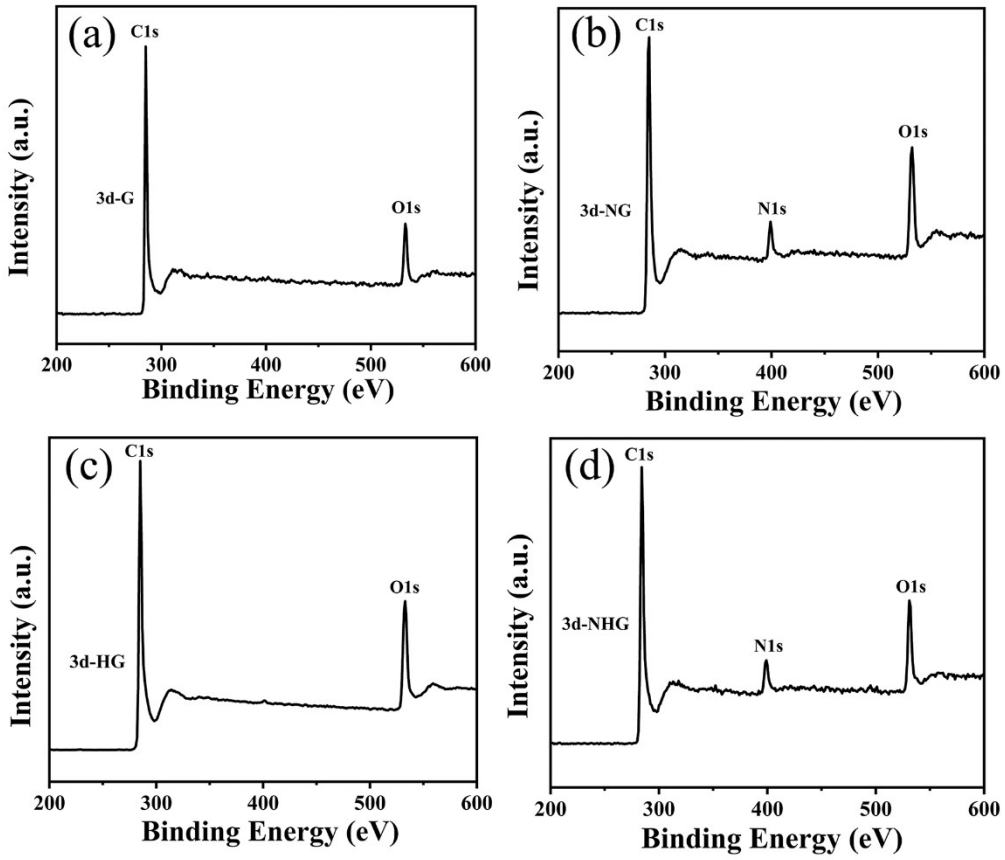

Figure S5. XPS (survey) spectrum of (a) 3d-G (b) 3d-NG (c) 3d-HG (d) 3d-NHG

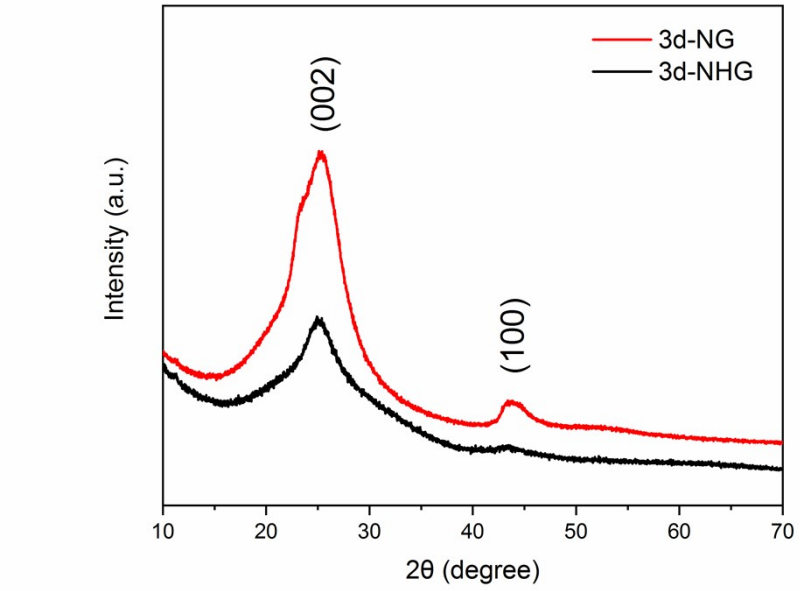

Figure S6. XRD patterns of 3d-NG and 3d-NHG.

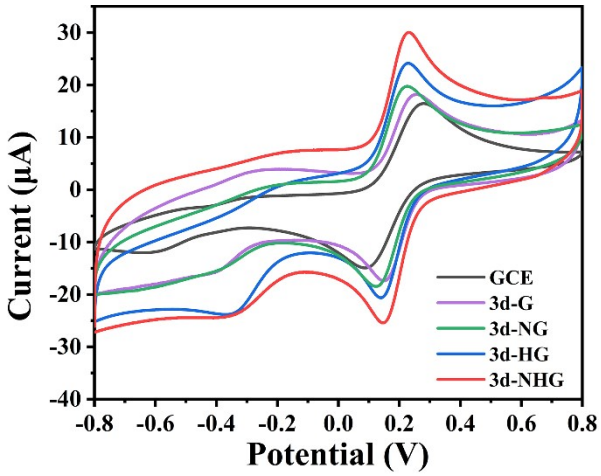

Figure S7. CV results of 1 mM $[Fe(CN)_6]^{3-/4-}$ and 0.1 M KCl solution on different modified GCEs at a scan rate of 50 mV s^{-1}.

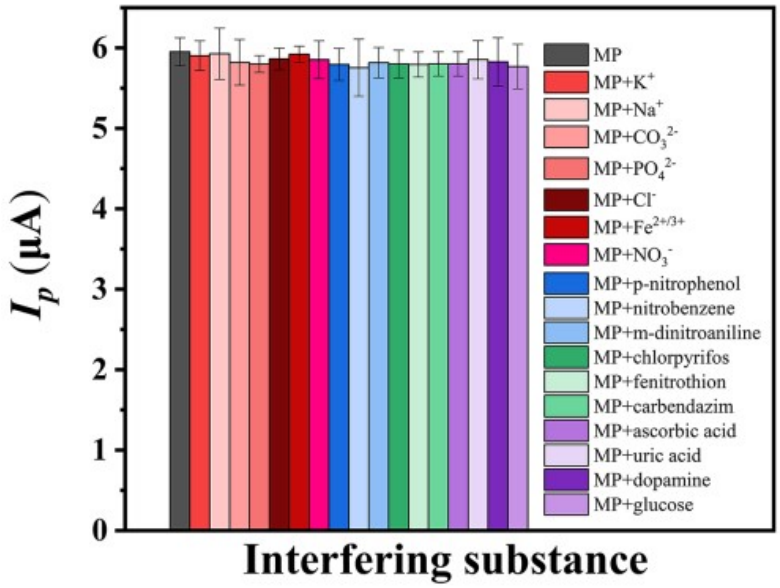

Figure S8. Selectivity of 3d-NHG/GCE for 8 μg·ml^{-1} MP versus inorganic ions (100-fold concentration), biological substances (10-fold concentration), nitro aromatic and pesticides compounds (1-fold concentration) in 0.1 M phosphate buffer (pH = 7).

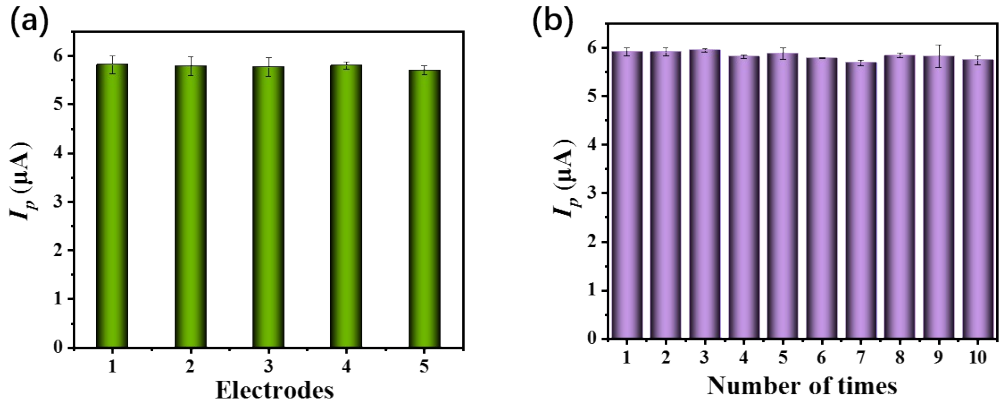

Figure S9. (a) Histograms of amperometric responses of the five electrodes, and (b) the same electrode for 10 repeat measurements of 8 μg·ml^{-1} MP in 0.1 M phosphate buffer (pH = 7).

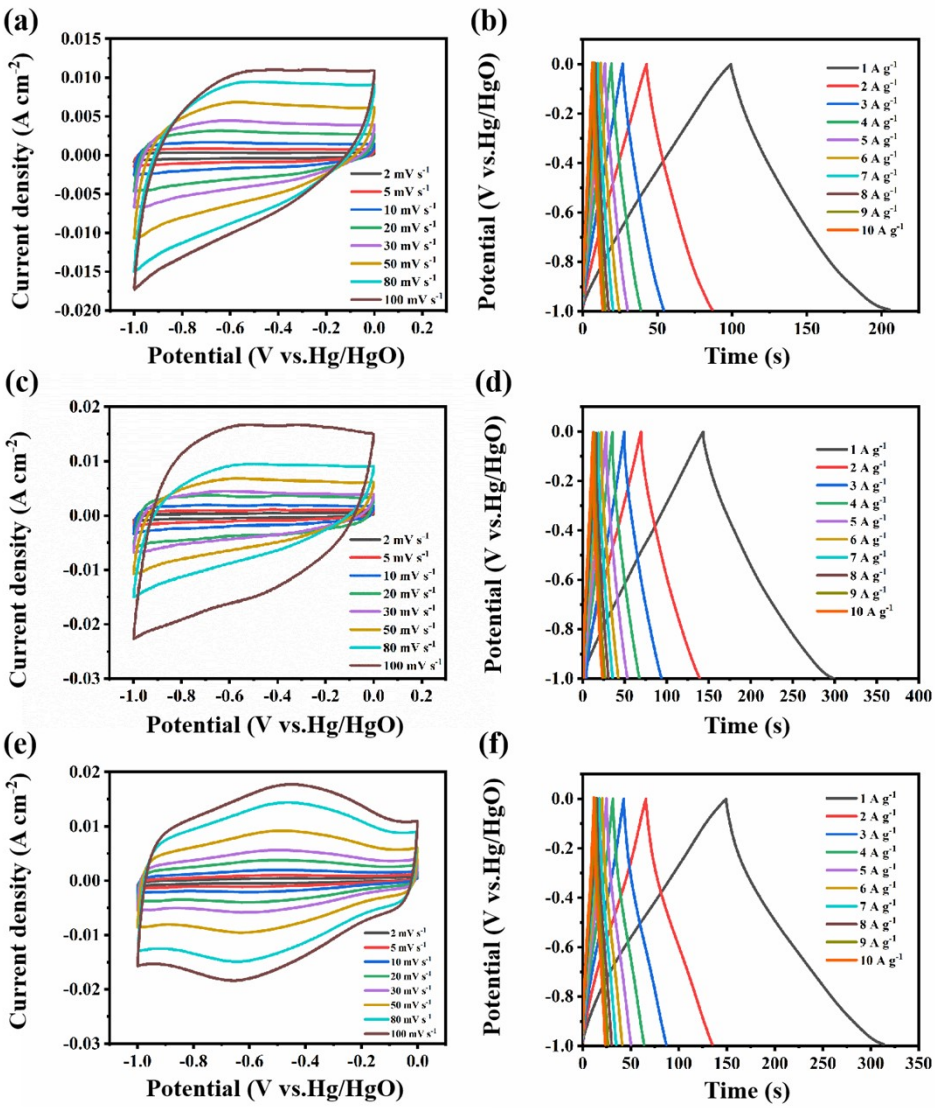

Figure S10. CV cures and GCD curves of (a, b) 3d-G, (c, d) 3d-NG, and (e, f) 3d-HG.

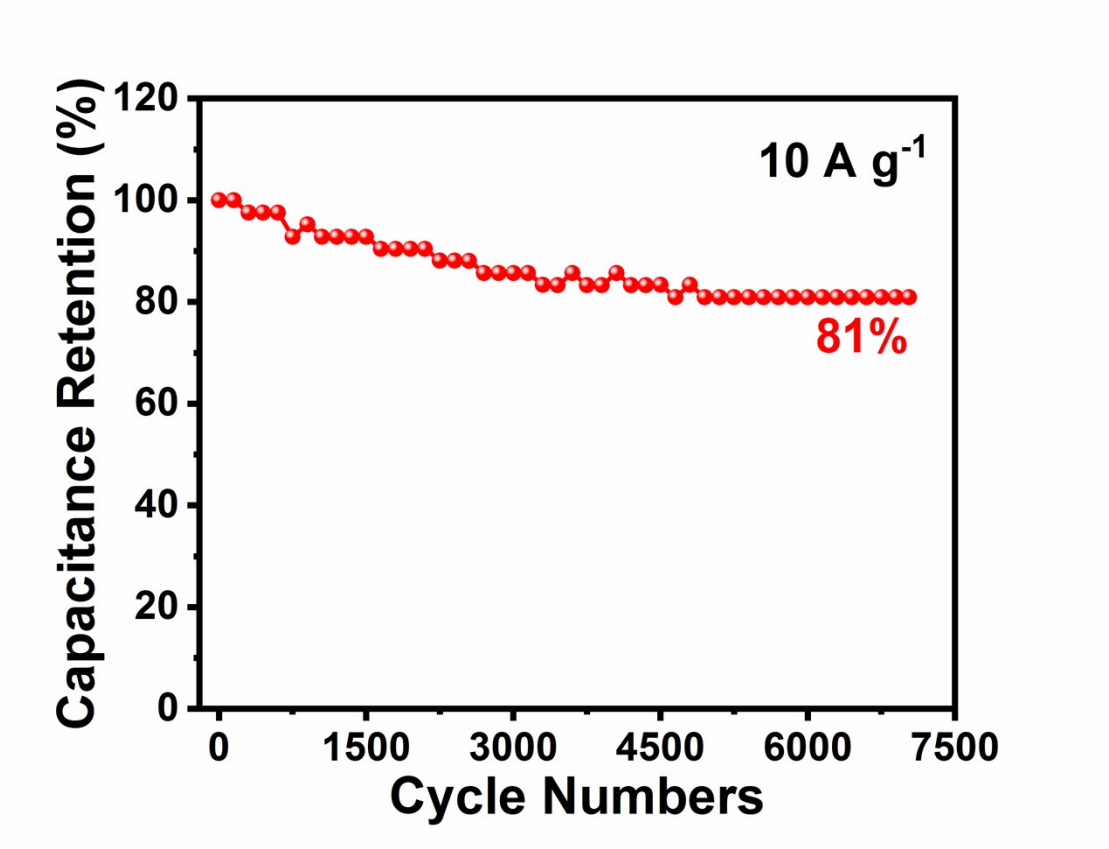

Figure S11. Cycle stability of 3d-NHG at 10 A g^{-1}.

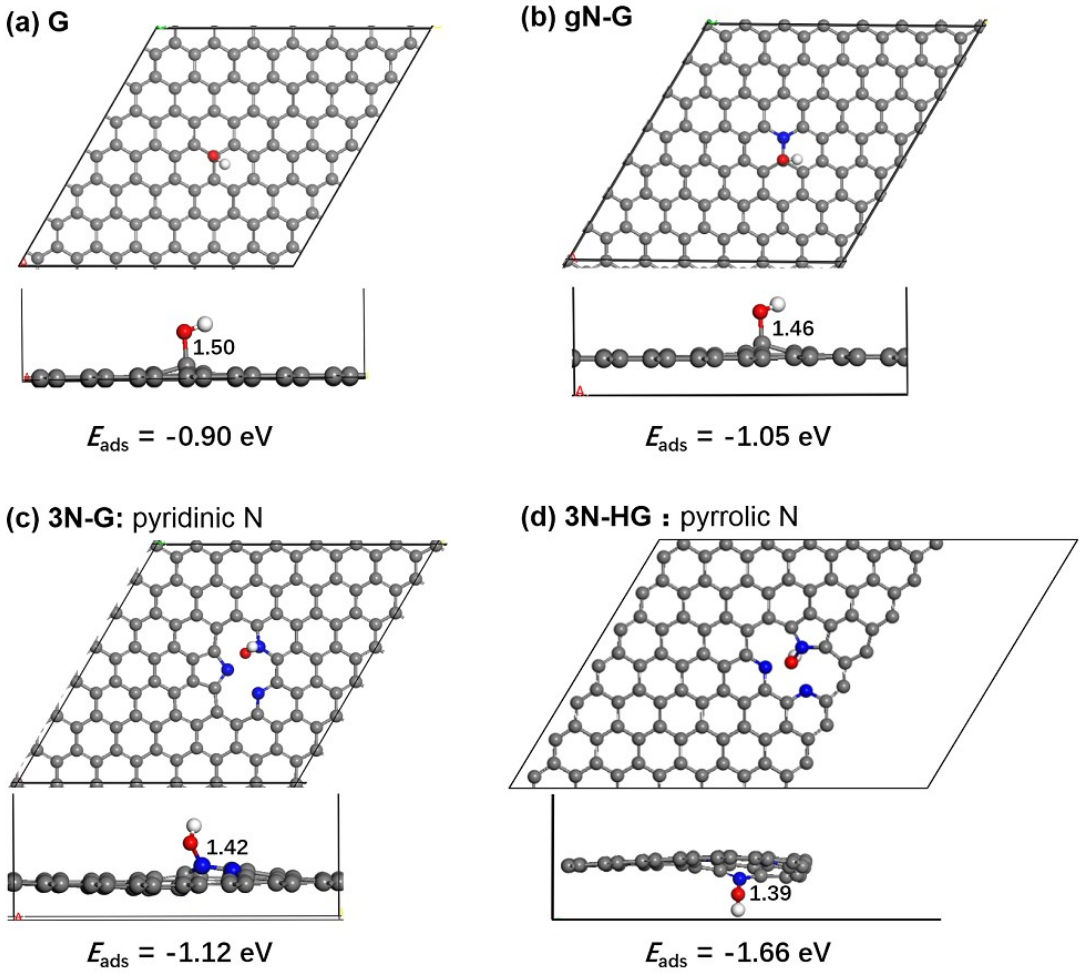

Figure S12. The most stable OH adsorption configuration on (a) graphene and (b) graphic N doped graphene and corresponding adsorption energy. (c) Optimized geometry of OH adsorption on (c) the pyridic N site of 3N-G and (e) the pyrrodic N site of 3N-HG and corresponding adsorption energy. The bond distance of O-N or O-C (in Å) is labeled.

Table S1 Comparison of different modified electrodes for MP determination

Electrode	Linear range	LOD (nM)	sensitivity (μA μM^{-1})	Reference
ZrO_2-CHIT/PEDOT/ITO	38 nM-7.6 μM	10.64	1.68	2
NPG/GCE	0.5-150 μM	20	13.06	3
Au-ZrO2-GNs/GCE	3.8 nM-9.12 μM	3.8	2.89	4
CuO-TiO_2	0-7.6 μM	4.60	5.98	5
CPME-AB	0.1-70 μM	39	0.76	6
3d-NHG/GCE	38 nM -570 μM	2.27	23.68	This work

Table S2 Results of the determination of MP in real samples

Real samples	Added (μg/ml)	Found (μg/ml)	Recovery (%)	RSD (n = 5, %)
Apples	0.5	0.504	100.8	2.47
	1.0	0.993	99.3	2.16
	1.5	1.503	100.2	1.15
River water	0.5	0.503	100.6	1.78
	1.0	1.045	104.5	1.62
	1.5	1.495	99.7	1.56

Table S3. The supercapacitor performance of the N-doped graphene compared with other N-doped carbonaceous materials.

Materials	Specific capacitance ($F\ g^{-1}$)	Capacitance retention	Ref.
3d-NHG	207 ($1\ A\ g^{-1}$)	76% ($10\ A\ g^{-1}$)	This work
CNT-N/S	172 ($1\ A\ g^{-1}$)	64% ($10\ A\ g^{-1}$)	7
CNT-N	97 ($1\ A\ g^{-1}$)	42% ($10\ A\ g^{-1}$)	7
NOHPC-650	185 ($1\ A\ g^{-1}$)	87% ($20\ A\ g^{-1}$)	8
N-HAC800	284 ($1\ A\ g^{-1}$)	64% ($20\ A\ g^{-1}$)	9
NGS-HMT-40	148 ($1\ A\ g^{-1}$)	95% ($4\ A\ g^{-1}$)	10
NDG-1	109 ($1\ A\ g^{-1}$)	93% ($2\ A\ g^{-1}$)	11
HTrGO-B	185 ($1\ A\ g^{-1}$)	92% ($10\ A\ g^{-1}$)	12
N-CNFs-900	202 ($1\ A\ g^{-1}$)	81% ($30\ A\ g^{-1}$)	13

References

1. J. Perdew *et al.* Generalized Gradient Approximation Made Simple. *Phys Rev Lett* **77**, (1996).
2. H. Zhou *et al.*, Poly 3,4-ethylenedioxythiophene and zirconia nanoparticles composite modified sensor for methyl parathion determination. *Journal of Electroanalytical Chemistry* **848**, (2019).
3. X. Gao, Y. Gao, C. Bian, H. Ma, H. Liu, Electroactive nanoporous gold driven electrochemical sensor for the simultaneous detection of carbendazim and methyl parathion. *Electrochimica Acta* **310**, 78-85 (2019).
4. N. Gao *et al.*, Electrochemical co-deposition synthesis of Au-ZrO_2-graphene nanocomposite for a nonenzymatic methyl parathion sensor. *Anal Chim Acta* **1072**, 25-34 (2019).
5. X. Tian *et al.*, Nonenzymatic electrochemical sensor based on CuO-TiO_2 for sensitive and selective detection of methyl parathion pesticide in ground water. *Sensors and Actuators B: Chemical* **256**, 135-142 (2018).
6. P. R. de Oliveira *et al.*, The use of activated biochar for development of a sensitive electrochemical sensor for determination of methyl parathion. *Journal of Electroanalytical Chemistry* **799**, 602-608 (2017).
7. F. Liu *et al.*, Influence of N/S Co-doping on Electrochemical Property of Brucite Template Carbon Nanotubes. *Journal of Inorganic Materials*, **36**, 711–717 (2021).
8 B. Yang *et al.*, Simple and green fabrication of a biomass-derived N and O self-doped hierarchical porous carbon via a self-activation route for supercapacitor application. *Carbon Letters*, **30**, 709–719 (2020).
9 D. Zeng *et al.*, Nest-like N-doped hierarchical porous active carbon formed by sacrifice template for enhanced supercapacitor. *Ionics*, **27**, 4461–4471 (2021).
10 J. W. Lee *et al.*, Hydrothermal preparation of nitrogen-doped graphene sheets via hexamethylenetetramine for application as supercapacitor electrodes *Electrochim Acta*, **85**, 459–466 (2012).
11 B. Jiang *et al.*, Highly concentrated, stable nitrogen-doped graphene for supercapacitors: Simultaneous doping and reduction. *Appl Surf Sci*, **258**, 3438–3443 (2012).
12 Y. Bai *et al.*, Effect of pH-induced chemical modification of hydrothermally reduced graphene oxide on supercapacitor performance. *J Power Sources*, **233**, 313–319 (2013).
13 L. F. Chen *et al.*, Synthesis of Nitrogen-Doped Porous Carbon Nanofibers as an Efficient Electrode Material for Supercapacitors. *ACS Nano*, **6**, 7092–7102 (2012).